Journal of Materials Chemistry C

PAPER

# Low temperature and high frequency effects on polymer-stabilized blue phase liquid crystals with large dielectric anisotropy

Cite this: J. Mater. Chem. C, 2014, 2, 3597

Fenglin Peng,[a] Yuan Chen,[a] Jiamin Yuan,[a] Haiwei Chen,[a] Shin-Tson Wu*[a] and Yasuhiro Haseba[b]

Received 17th January 2014
Accepted 19th February 2014

DOI: 10.1039/c4tc00115j

www.rsc.org/MaterialsC

We report the low temperature and high frequency effects on polymer-stabilized blue phase liquid crystals (BPLCs) comprising of a large dielectric anisotropy nematic host. Debye dielectric relaxation sets a practical limit even when the device operation temperature is still within the blue phase range. To explain these phenomena, we propose a model to describe the temperature and frequency dependent Kerr constant and obtain excellent agreement with experiment. Doping a diluter compound to the BPLC host helps to reduce viscosity, which in turn boosts the dielectric relaxation frequency and extends the low temperature operation range.

## Introduction

After about one decade of extensive material research and device structure development, the major technical barriers preventing polymer-stabilized blue phase liquid crystals (PS-BPLCs)[1–4] from widespread applications have been gradually overcome. The operation voltage has been reduced from 50 V to 10 V by employing a large dielectric anisotropy ($\Delta\varepsilon > 100$) BPLC material[5,6] and implementing a device with protruded or etched electrodes.[7–10] Transmittance higher than 80% can be achieved by optimizing the refraction effect of the non-uniform fringing electric fields.[11] Hysteresis can be greatly suppressed by reducing the peak electric field near the edges of electrodes,[12] using vertical field switching,[13] adding nanoparticles,[14–16] or controlling the UV exposure conditions.[17] The dawn of BPLCs era seems near.

However, for a mobile display or photonic device, low temperature and high frequency operations are critical issues, especially for outdoor applications or color sequential displays using red, green and blue LEDs.[18,19] Generally speaking, the ultimate low temperature operation of a BPLC device is limited by its phase transition temperature, but in this paper we find that Debye relaxation of these large $\Delta\varepsilon$ BPLC materials sets another practical limit. Due to submillisecond gray-to-gray response time,[6,20] BPLCs are ideally suited for color sequential displays. By eliminating spatial color filters, both optical efficiency and resolution density can be tripled. However, to achieve field sequential colors without seeing annoying color breakup, the required frame rate should be tripled. For example, if a spatial color-filter-based LC device is operated at 120 Hz, then the temporal color sequential LC should be operated at 360 Hz or higher. For a large $\Delta\varepsilon$ BPLC, its Debye relaxation frequency is as low as 1.3 kHz.[6,21] Therefore, if the driving frequency gets close to the Debye relaxation frequency of the BPLC, then the Kerr constant would decrease dramatically, which in turn demands for a very high operation voltage. This sets another practical limit from the viewpoint of device operation.

In this paper, we report the low temperature and high frequency operation limits of BPLC devices. To correlate the electro-optic properties of the BPLC with its LC host, we propose a physical model to describe the temperature and frequency dependent Kerr constant. The model fits well with our experimental data. To increase the Debye relaxation frequency, we dope a diluter compound to the BPLC host, which greatly extends the low temperature and high frequency operation limits.

## Experimental and results

In experiment, we prepared two BPLC samples employing JC-BP06N and JC-BP07N (from JNC) as LC hosts. The dielectric anisotropy at low frequency limit of JC-BP06N is 648, which is almost twice of JC-BP07N ($\Delta\varepsilon \sim 332$). The BPLC precursors are comprised of 88.17 wt% LC host (JC-BP06N or JC-BP07N), 2.92 wt% chiral dopant R5011 (from HCCH, China), 8.70 wt% monomers (5.24 wt% RM257 from Merck and 3.46 wt% TMPTA (1,1,1-trimethylolpropane triacrylate, from Sigma-Aldrich)) and 0.21 wt% photoinitiator. These samples were filled into two in-plane-switching (IPS) cells whose electrode width is 8 μm, electrode gap is 12 μm, and cell gap is 7.34 μm. The IPS cells were coated with a thin indium tin oxide (ITO) film, but without any surface

[a]College of Optics and Photonics, University of Central Florida, Orlando, Florida, USA. E-mail: swu@ucf.edu; Fax: +1-407-823-6880; Tel: +1-407-823-4763
[b]JNC Petrochemical Corporation, Ichihara Research Center, Ichihara, Chiba 290-8551, Japan

alignment layer. Both cells were cooled to the BP-I phase and cured by UV light with wavelength $\lambda \sim 365$ nm and intensity $\sim 2$ mW cm$^{-2}$ for 30 min. After UV curing, the PS-BPLC cells were quite clear because their Bragg reflections were in the UV region. For convenience, we call these two cells as PSBP-06 and PSBP-07. Next, both cells were placed on a Linkam heating stage controlled by using the temperature program (Linkam TMS94). We measured the voltage-dependent transmittance (VT) by sandwiching the heating stage between two crossed polarizers. A He–Ne laser ($\lambda = 633$ nm) was used as a probing beam and the transmitted light was focused by a lens, so that different diffraction orders can be collected by using the detector.[22]

When a LC cell is subject to an external voltage, the LC directors respond to the root-mean-square voltage ($V_{rms}$). In a thin-film-transistor (TFT) LCD, the driving waveform is square waves. But for studying the frequency effect, a sinusoidal wave is preferred because a square wave contains multiple Fourier frequency components. Therefore, we first compare the difference between these two driving waveforms. We measured the VT curves of PSBP-06 and PSBP-07 at room temperature (RT = 22 °C) and several frequencies: $f = 120$ Hz, 240 Hz, 480 Hz, 720 Hz and 1 kHz (both sinusoidal wave and square wave AC voltage). It is known that under the same frequency, the root-mean-square voltage of a sine wave is $\sqrt{2}$ larger than that of a square wave.

Fig. 1 shows the measured VT curves of PSBP-07 at $f = 480$ Hz and $\lambda = 633$ nm. The blue and black curves represent the data with square wave and sine wave voltages, respectively. If we divide the data points of the black curve by $\sqrt{2}$, the dotted red curve overlaps with the blue curve reasonably well. Similar results are found for other frequencies and PSBP-06. Therefore, the VT curves for square waves and sine waves are consistent except their magnitude is different by a factor of $\sqrt{2}$. To simulate TFT operation, from here on we will use square wave RMS voltage, unless otherwise mentioned.

Next, we studied the temperature effects. Fig. 2 shows the normalized VT curves of PSBP-06 measured from 40 °C to 0 °C at $f = 480$ Hz. As the temperature ($T$) decreases, the VT curves shift leftward first and then rightward, indicating $V_{on}$ bounces back at low temperatures. The lowest $V_{on}$ occurs at ~20 °C. As the temperature drops to 3 °C, which is still above the melting point of PSBP-06 ($T_{mp} = -2$ °C), the transmittance stays below 5% (normalized to the peak transmittance at 60 Hz under the same temperature) even the applied voltage has reached 65 $V_{rms}$. Therefore, this imposes a practical low temperature operation limit for PSBP-06. A similar phenomenon was also observed for PSBP-07. We will further discuss this temperature limit later.

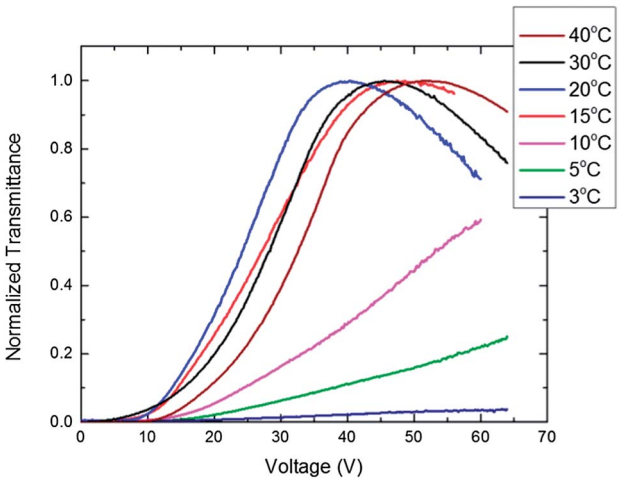


Fig. 2 Measured VT curves of PSBP-06 at the specified temperatures. $f = 480$ Hz and $\lambda = 633$ nm.

## Physical mechanisms

We fit each VT curve for both cells with an extended Kerr effect model[23] and plot the obtained $K$ values in Fig. 3. In an isotropic state (left side), *i.e.*, $T > T_c$ (clearing point), the Kerr constant vanishes ($K \approx 0$). As the temperature decreases from $T_c$, $K$ increases linearly with $\sim 1/T$, gradually reaching a maximum, and then declines steeply. Let us call the temperature where maximum $K$ occurs as optimal operation temperature, $T_{op}$. In the $T_c < T < T_{op}$ region, our results agree well with the model

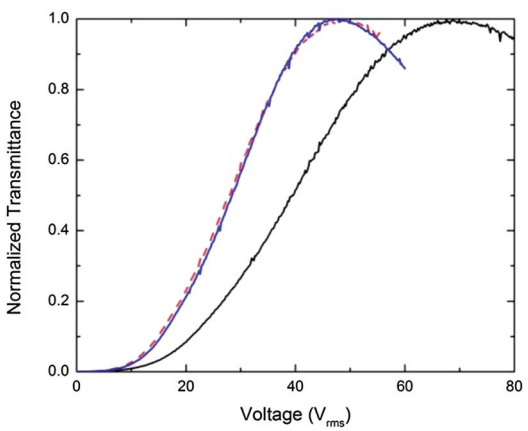


Fig. 1 Measured VT curves of PSBP-07 at $f = 480$ Hz, $\lambda = 633$ nm, and RT. Black curve: sine waves, blue curve: square waves, and dashed lines: black curve divided by $\sqrt{2}$.

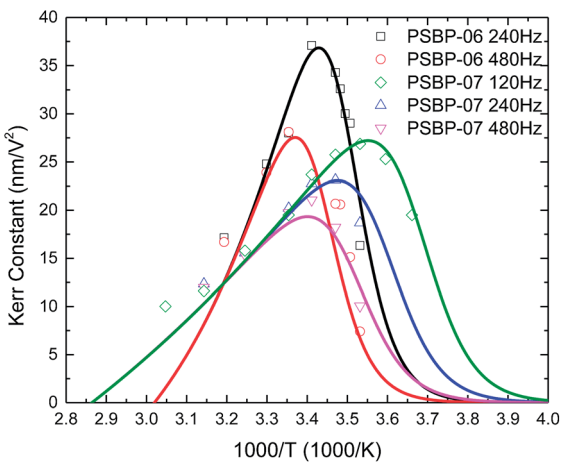


Fig. 3 Temperature dependent Kerr constants of PSBP-06 at $f =$ 240 Hz, 480 Hz and PSBP-07 at $f = 120$ Hz, 240 Hz and 480 Hz separately. Lines represent fitting curves with eqn (9).

published by Rao *et al.*[24] and Tian *et al.*,[25] but the sharp plunge of the Kerr constant when $T_{op} < T$ has not been reported previously. From Fig. 3, $T_{op}$ depends on the BPLC material and frequency.

To better understand the observed phenomena, we analyze the temperature and frequency effects on Kerr constant. Based on Gerber's model,[26] $K$ is governed by the birefringence ($\Delta n$), average elastic constant ($k$), $\Delta\varepsilon$ and pitch length ($P$) of the chiral LC host as:

$$K \sim \frac{\Delta n \varepsilon_o \Delta\varepsilon P^2}{k_B \lambda (2\pi)^2} \quad (1)$$

Here $\Delta n$, $k$, and $\Delta\varepsilon$ are all temperature dependent, as described by the following relationship:[22,27,28]

$$\Delta n \sim \Delta n_o S, \quad (2)$$

$$\Delta\varepsilon \sim S \exp(E_1/k_B T), \quad (3)$$

$$k \sim S^2, \quad (4)$$

$$S = (1 - T/T_{cn})^{\beta}, \quad (5)$$

where $S$ denotes the order parameter, $\Delta n_o$ is the extrapolated birefringence at $T = 0$ K, $E_1$ is a parameter related to the dipole moment, $k_B$ is the Boltzmann constant, $T_{cn}$ is the clearing point of the nematic host and $\beta$ is a material constant. On the other hand, the pitch length ($P$) is not sensitive to the temperature.[29] Substituting eqn (2)–(4) in eqn (1), we find that $K \sim \exp(E_1/k_B T)$. Generally speaking, as the temperature increases $K$ decreases. From eqn (1), the frequency effect of $K$ originates from $\Delta\varepsilon$ because the remaining parameters are all independent of frequency in the low frequency region. Based on the Debye relaxation model, $\Delta\varepsilon$ has the following form:[30]

$$\Delta\varepsilon = \Delta\varepsilon_\infty + \frac{\Delta\varepsilon_o - \Delta\varepsilon_\infty}{1 + (f/f_r)^2}, \quad (6)$$

where $\Delta\varepsilon_\infty$ and $\Delta\varepsilon_o$ are the dielectric anisotropy at high and low frequency limits respectively, $f$ is the operation frequency, and $f_r$ is the relaxation frequency. For a low viscosity nematic LC host, its $f_r$ is usually over 100 kHz, which is much higher than the intended operation frequency (*e.g.*, 120–960 Hz) of the LC device. As a result, the $f/f_r$ term in eqn (6) can be neglected and $\Delta\varepsilon \approx \Delta\varepsilon_o$, which is insensitive to the frequency. However for a large $\Delta\varepsilon$ BPLC, the bulky molecules cannot follow the electric field in the high frequency region. The Debye relaxation frequency is usually in the 1–2 kHz region. Thus, the $f/f_r$ term in eqn (6) becomes significant. As a result, $\Delta\varepsilon$ (or Kerr constant) is strongly dependent on the frequency.

In the experiment, we measured the capacitance of a homogeneous cell and a homeotropic cell using an HP-4274 multi-frequency LCR meter (sine waves) to determine the $\Delta\varepsilon$ of JC-BP06N and JC-BP07N at different temperatures.[27] Fig. 4 depicts the measured $\Delta\varepsilon$ (dots) and fitting curve (solid lines) with eqn (6) for JC-BP06N. Through fittings, $f_r$ at each temperature is obtained. The results indicate that $f_r$ decreases exponentially with $T$ as:[31]

$$f_r = f_o \exp(-E_2/k_B T). \quad (7)$$

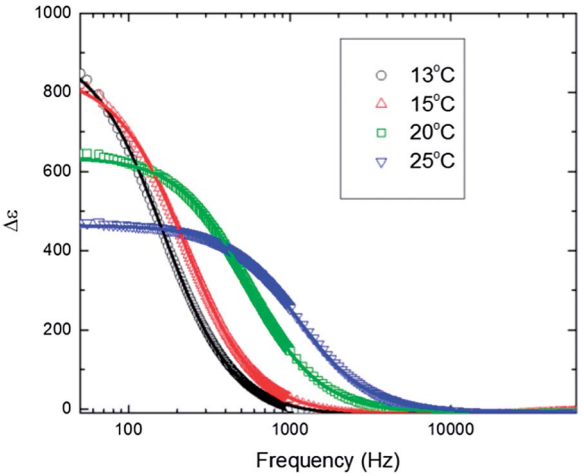


Fig. 4 Frequency dependent $\Delta\varepsilon$ of JC-BP06N at the four specified temperatures. Dots are measured data and lines are fittings with eqn (6).

here $E_2$ is the activation energy of molecular rotation and $f_o$ is a proportionality constant. From eqn (6) and (7), once $f$ gets close to $f_r$, $\Delta\varepsilon$ decreases as $T$ decreases because the ratio of $f/f_r$ increases. As shown in Fig. 4, at 480 Hz $\Delta\varepsilon$ decreases by ~2× as $T$ decreases from 20 °C to 13 °C. This explains well why $V_{on}$ 'bounces back' as the temperature decreases [Fig. (2)]. Substituting eqn (3), (6) and (7) in eqn (1), the Kerr constant can be expressed as:

$$K \sim A \frac{\exp(E_1/k_B T)}{1 + (f/f_r)^2} = A \frac{\exp(E_1/k_B T)}{1 + (f/f_o)\exp(E_2/k_B T)^2}, \quad (8)$$

where $A$ is a proportionality constant. However, when the temperature approaches $T_c$ both $\Delta n$ and $\Delta\varepsilon$ vanish, so does the Kerr constant (at least dramatically decreased). To satisfy these boundary conditions, we modify eqn (8) as follows:

$$K = A \frac{\exp\left[\frac{E_1}{k_B}\left(\frac{1}{T} - \frac{1}{T_C}\right)\right] - 1}{1 + (f/f_o)\exp(E_2/k_B T)^2} \quad (9)$$

We fitted $K$ at various temperatures with eqn (9) for both PSBP-06 and PSBP-07. Good agreement is obtained as depicted in Fig. 3. Eqn (9) involves 4 unknowns, but $f_o$ and $E_2$ can be found by fitting the relaxation frequency, as eqn (7) indicates. Through fitting the temperature dependent Kerr constant at a given frequency, we can obtain $A$ and $E_1$. The fitting parameters are listed below. For PSBP-06, $f_o = 9.76 \times 10^{18}$ Hz, $E_1 = 281.0$ meV, $A = 16.54$ nm V$^{-2}$, $E_2 = 945.1$ meV, and for PSBP-07, $f_o = 4.80 \times 10^{15}$ Hz, $E_1 = 74.8$ meV, $A = 37.65$ nm V$^{-2}$, and $E_2 = 736.1$ meV.

In principle, we can derive the analytical form of optimal operation temperature ($T_{op}$) by solving $\frac{\partial K}{\partial T} = 0$, but it is too complicated to present it here. Generally, $T_{op}$ is governed by several parameters listed in eqn (9), such as frequency, relaxation frequency, temperature, *etc.* From Fig. 2, the $T_{op}$ of PSBP-06 at 240 Hz and 480 Hz is at 18.8 °C and 22.5 °C, respectively.

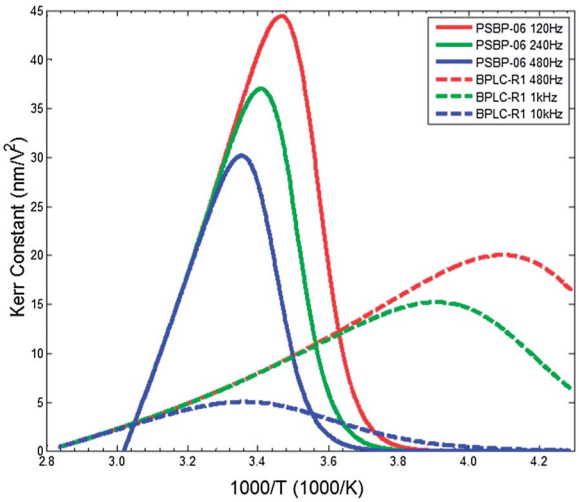


Fig. 5 Temperature dependent Kerr constant of PSBP-06 ($f_r \sim 1.2$ kHz) and BPLC-R1 ($f_r \sim 15$ kHz) at the specified frequencies, $\lambda = 633$ nm.

Ideally, we would like to design a BPLC with its $T_{op}$ (or highest Kerr constant) located at the intended operation frequency and temperature. Therefore, we investigated the frequency effect on $T_{op}$ in more detail.

Fig. 5 depicts the temperature dependent Kerr constant at different frequencies for two PSBP composites: PSBP-06 and BPLC-R1. The latter has a smaller Kerr constant because its LC host has a smaller $\Delta\varepsilon$ (~50), but its viscosity is also much lower than that of JC-BP06N. The $f_r$ of the BPLC-R1 host is ~15 kHz at 25 °C, which is ~10× higher than that of JC-BP06N. For the two BPLC samples shown in Fig. 5, the RGB curves (representing low, medium and high frequencies for each sample) overlap in the high temperature region, which means their Kerr constant is proportional to $1/T$, but is quite insensitive to the frequency. This can be explained as follows. In the high temperature region, the BPLC has a lower viscosity so that its relaxation frequency is higher [eqn (7)]. From eqn (8), when $f_r \gg f$ the frequency part can be ignored and $K$ is inert to the frequency. As the temperature decreases (or $1/T$ increases), $f_r$ decreases exponentially [eqn (7)]. The blue curve (whose $f$ is closer to $f_r$) bends down first due to the dramatically reduced $\Delta\varepsilon$ [Fig. 4]. As a result, its maximum Kerr constant is smaller, which leads to a higher operation voltage. For the green and red curves, their corresponding frequency is lower so that their peak Kerr constant and bending over phenomenon occur at a lower temperature, as depicted in Fig. 5.

For a given BPLC, its $T_{op}$ increases as the frequency increases. Let us illustrate this using PSBP-06 as an example. In Fig. 5, as the frequency increases from 120 Hz to 480 Hz, the $T_{op}$ increases gradually from 15.0 °C to 22.5 °C, but in the meantime the Kerr constant decreases from 44.4 nm V$^{-2}$ to 30.1 nm V$^{-2}$. If the relaxation frequency of a BPLC is too high, then its $T_{op}$ might shift outside the intended operation temperature range. Let us take BPLC-R1 as an example: at 480 Hz its $T_{op}$ occurs at −30 °C, as shown in Fig. 5. At such a low operation temperature, the viscosity of the BPLC would increase dramatically. If we want to shift $T_{op}$ to room temperature, then the operation frequency should be increased to ~10 kHz, which would increase the power consumption dramatically. An optimal relaxation frequency should be in the 2–3 kHz range.

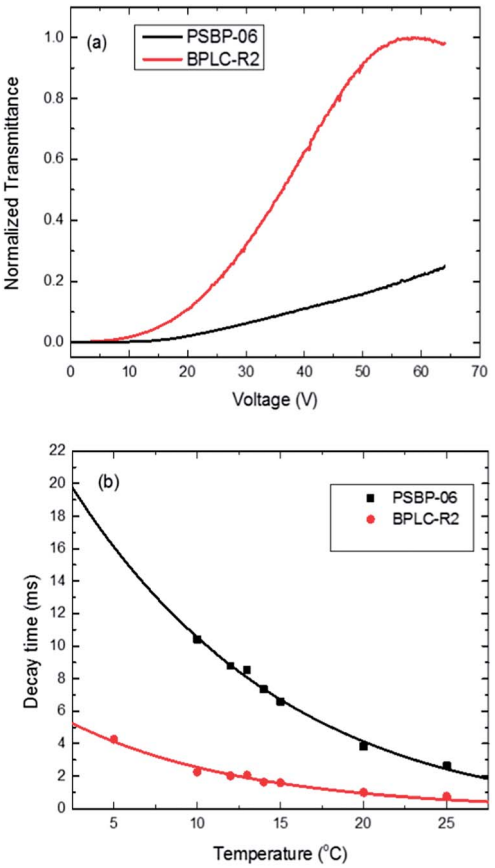


Fig. 6 (a) Measured VT curves of PSBP-06 and BPLC-R2 at 5 °C with $f$ = 480 Hz and $\lambda$ = 633 nm; (b) temperature dependent response time of PSBP-06 and BPLC-R2. Dots are measured data and solid lines represent fittings with eqn (7) of ref. 5.

## Diluter effect

Melting point sets the ultimate low temperature operation limit for a BPLC device. However, in this study we find another factor which limits the practical applications. Even the temperature is still above the melting point of a blue phase, the dramatic plunge of $\Delta\varepsilon$ makes the device difficult to operate, which seriously limits the usefulness of the device. Let us take PSBP-06 as an example. As the temperature decreases from 25 °C to 5 °C, the transmittance remains so low even the voltage has reached 65 $V_{rms}$ [Fig. 2] and the decay time increases exponentially to 17 ms. These problems could hinder the BPLC application in low temperatures. The abrupt decrease in the Kerr constant is because the relaxation frequency is too low.

To raise the relaxation frequency, doping a diluter compound has been proven to be quite effective.[32] The relaxation frequency $f_r$ is proportional to the average molecular length ($l$) and viscosity $\eta$ as $f_r \sim \frac{1}{\eta l^3}$.[33] Doping a low molecular weight, short-chain and low viscosity diluter to a bulky BPLC host would

increase the relaxation frequency noticeably. In the experiment, we doped 13 wt% 5CC3 [4-pentyl-4′-propyl-1,1′-bi(cyclohexyl)] into the JC-BP06N host, which shifts $f_r$ from 1.1 kHz to 4.85 kHz at 25 °C. We call this new mixture as BPLC-R2. Although the $V_{on}$ of BPLC-R2 is somewhat higher than that of PSBP-06 at 25 °C, its performance in the low temperature region is much better than that of PSBP-06. Fig. 6(a) depicts the measured VT curves and Fig. 6(b) shows the measured response time at 5 °C. With a diluter, both $V_{on}$ and decay time decreased significantly. Therefore, a good diluter helps to maintain the high performance of BPLCs in the low temperature region.

## Conclusions

We have developed a physical model to correlate the temperature and frequency effects on the Kerr constant of BPLC materials. The model fits very well with the experimental data. Based on the model, we find that for a given BPLC material and frequency, there exists an optimal operation temperature where the Kerr constant has a maximum value, or $V_{on}$ is the lowest. Although the melting point of a BPLC sets its ultimate operation limit, we found another practical limit which originates from the Debye relaxation of dielectric anisotropy at low temperatures. Doping a diluter to a BPLC host helps to extend the low temperature operation limit.

## Acknowledgements

The authors are indebted to Industrial Technology Research Institute (ITRI), Taiwan, for the financial support, and Yifan Liu and Jing Yan for helpful discussions.

## References and notes

1 H. Kikuchi, M. Yokota, Y. Hisakado, H. Yang and T. Kajiyama, *Nat. Mater.*, 2002, **1**, 64.
2 Y. Hisakado, H. Kikuchi, T. Nagamura and T. Kajiyama, *Adv. Mater.*, 2005, **17**, 96.
3 J. Yan and S. T. Wu, *Opt. Mater. Express*, 2011, **1**, 1527.
4 J. Yan, L. Rao, M. Jiao, Y. Li, H. C. Cheng and S. T. Wu, *J. Mater. Chem.*, 2011, **21**, 7870.
5 L. Rao, J. Yan, S. T. Wu, S. Yamamoto and Y. Haseba, *Appl. Phys. Lett.*, 2011, **98**, 081109.
6 Y. Chen, D. Xu, S. T. Wu, S. Yamamoto and Y. Haseba, *Appl. Phys. Lett.*, 2013, **102**, 141116.
7 M. Jiao, Y. Li and S. T. Wu, *Appl. Phys. Lett.*, 2010, **96**, 011102.
8 L. Rao, Z. Ge and S. T. Wu, *J. Disp. Technol.*, 2010, **6**, 115.
9 S. Yoon, M. Kim, M. S. Kim, B. G. Kang, M. K. Kim, A. K. Srivastava, S. H. Lee, Z. Ge, L. Rao, S. Gauza and S. T. Wu, *Liq. Cryst.*, 2010, **37**, 201.
10 M. Kim, M. S. Kim, B. G. Kang, M. K. Kim, S. Yoon, S. H. Lee, Z. Ge, L. Rao, S. Gauza and S. T. Wu, *J. Phys. D: Appl. Phys.*, 2009, **42**, 235502.
11 D. Xu, Y. Chen, Y. Liu and S. T. Wu, *Opt. Express*, 2013, **21**, 24721.
12 L. Rao, J. Yan, S. T. Wu, Y. C. Lai, Y. H. Chiu, H. Y. Chen, C. C. Liang, C. M. Wu, P. J. Hsieh, S. H. Liu and K. L. Cheng, *J. Disp. Technol.*, 2011, **7**, 627.
13 H. C. Cheng, J. Yan, T. Ishinabe and S. T. Wu, *Appl. Phys. Lett.*, 2011, **98**, 261102.
14 L. Wang, W. He, X. Xiao, M. Wang, M. Wang, P. Yang, Z. Zhou, H. Yang, H. Yu and Y. Lu, *J. Mater. Chem.*, 2012, **22**, 19629.
15 L. Wang, W. He, X. Xiao, Q. Yang, B. Li, P. Yang and H. Yang, *J. Mater. Chem.*, 2012, **22**, 2383.
16 L. Wang, W. He, Q. Wang, M. Yu, X. Xiao, Y. Zhang, M. Ellahi, D. Zhao, H. Yang and L. Guo, *J. Mater. Chem. C*, 2013, **1**, 6526.
17 T. N. Oo, T. Mizunuma, Y. Nagano, H. Ma, Y. Ogawa, Y. Haseba, H. Higuchi, Y. Okumura and H. Kikuchi, *Opt. Mater. Express*, 2011, **1**, 1502.
18 S. Gauza, X. Zhu, W. Piecek, R. Dabrowski and S. T. Wu, *J. Disp. Technol.*, 2007, **3**, 250.
19 M. Kobayashi, A. Yoshida and Y. Yoshida, *SID Int. Symp. Dig. Tech. Pap.*, 2010, **41**, 1434.
20 K. M. Chen, S. Gauza, H. Xianyu and S. T. Wu, *J. Disp. Technol.*, 2010, **6**, 49.
21 Y. Li, Y. Chen, J. Sun, S. T. Wu, S. H. Liu, P. J. Hsieh, K. L. Cheng and J. W. Shiu, *Appl. Phys. Lett.*, 2011, **99**, 181126.
22 J. Yan, Y. Chen, S. T. Wu and X. Song, *J. Disp. Technol.*, 2013, **9**, 24.
23 J. Yan, H. C. Cheng, S. Gauza, Y. Li, M. Jiao, L. Rao and S. T. Wu, *Appl. Phys. Lett.*, 2010, **96**, 071105.
24 L. Rao, J. Yan and S.-T. Wu, *J. Soc. Inf. Disp.*, 2010, **18**, 954.
25 L. Tian, J. W. Goodby, V. Görtz and H. F. Gleeson, *Liq. Cryst.*, 2013, **40**, 1446.
26 P. R. Gerber, *Mol. Cryst. Liq. Cryst.*, 1985, **116**, 197.
27 S. T. Wu and C. S. Wu, *Phys. Rev. A*, 1990, **42**, 2219.
28 S. T. Wu, *Phys. Rev. A*, 1986, **33**, 1270.
29 F. Zhang and D. K. Yang, *Liq. Cryst.*, 2002, **29**, 1497.
30 H. Xianyu, S. T. Wu and C. L. Lin, *Liq. Cryst.*, 2009, **36**, 717.
31 M. Schadt, *J. Chem. Phys.*, 1972, **56**, 1494.
32 Y. Chen, J. Yan, M. Schadt, S. H. Liu, K. L. Cheng, J. W. Shiu and S. T. Wu, *J. Disp. Technol.*, 2013, **9**, 592.
33 L. M. Blinov, *Electro-optical and magneto-optical properties of liquid crystals*, Wiley, 1983.